



Spatiotemporal variability of the relationship between seasonal temperatures and precipitation in Spain, 1951–2019

F. S. Rodrigo¹

Received: 22 February 2023 / Accepted: 23 June 2023 / Published online: 28 June 2023
© The Author(s), under exclusive licence to Springer-Verlag GmbH Austria, part of Springer Nature 2023

Abstract

This paper studies the spatiotemporal variability of the IR_t index (defined as the difference between the percentage of precipitation corresponding to warm days and cold days in year t) calculated at 35 stations in the Iberian Peninsula during 1951–2019. Spatial variability is estimated using cluster analysis (Euclidean distance, Ward's method), which allows regionalization of the data set for each year's season. For each cluster, the $\langle IR \rangle$ index is defined as the average of the indexes corresponding to each cluster element. The temporal evolution of the $\langle IR \rangle$ indices is analyzed by studying the appearance of trends using the Mann–Kendall test and the possible existence of various subperiods using the cumulative sum of deviations and the t-test for the difference between the means. The role of EA, EA/WR, NAO, SCAN and WeMO teleconnection patterns in modulating the relationship between temperature and precipitation is analyzed by applying multiple regression analysis. The results show a trend towards positive (or less negative) values in the relationship between temperatures and precipitation (of varying magnitude depending on the region and season) and the contribution of atmospheric dynamics to these changes.

1 Introduction

A recent paper (Blöschl et al. 2020) highlights that in the last 500 years, there has been a change in the flood frequency pattern in various regions of Europe. While historically, floods occurred in cooler-than-usual phases, the most recent high flood frequency period (1990–2016) is characterized by warmer thermal attributes. Yang et al. (2021) indicate a transition from warm-dry to warm-humid conditions in the eastern area of northwest China starting in the 1990s. Furthermore, Kim et al. (2017) find changes in forward-looking projections of seasonal temperature-precipitation correlations in Korea and Northwestern Europe. These results seem to indicate a change in the relationship between temperature and precipitation since the end of the twentieth century. It is interesting, therefore, to study the joint variability of temperature and precipitation and analyze possible changes in the collective behavior of both variables.

The relationship between temperatures and precipitation is not simple. Depending on the geographical area and season, several physical processes can determine whether this

relationship is positive or negative (Du et al. 2013). The primary relationship between temperature and precipitation is a consequence of the laws of thermodynamics, such as that of Clausius-Clapeyron, the transfer of sensible and latent heat during phase changes of water within clouds and at the land surface, and the radiative properties of the different subsystems of the climate system (Trenberth 2011). Numerous studies have focused on analyzing this problem from different methodological perspectives, both globally and regionally (see, for example, Beniston 2009; Dobrinsky et al. 2018; Lazoglou and Anagnostopoulou 2019; Hao et al. 2020; Chen et al. 2022; Dong et al. 2021; Pinskiwar 2022). In addition, other factors may influence this relationship, such as surface pressure, wind intensity and atmospheric circulation (Berg et al. 2015). We can therefore distinguish between the thermodynamic and dynamic components in the relationship between the two variables (Cheng et al. 2018). In this context, it makes sense to ask about atmospheric dynamics' contribution to climate variables changes (van Haren et al. 2015; Zappa 2019; Suárez-Gutiérrez et al. 2020).

In a previous work (Rodrigo 2022), the IR_t index was defined as a simple measure of the relationship between temperature and precipitation. A positive IR_t index indicates warm-humid or, alternatively, cold-dry conditions, while a negative IR_t index would indicate the opposite situation (warm-dry or cold-humid conditions). The IR_t

✉ F. S. Rodrigo
frodrigo@ual.es

¹ Dept. Chemistry and Physics, University of Almería, La Cañada de San Urbano, S/N, 04120 Almería, Spain

index is a modified version of the TPI index defined by Isaac and Stuart (1992). The TPI index is defined as the percentage of precipitation occurring at daily temperatures lower than the median of the temperature series. A percentage lower than 50% indicates that precipitation and warm days occur together, while the opposite would occur with percentages higher than 50%. This index is advantageous because it can be applied to stations with a climatic record limited to the magnitudes of mean daily temperature and total daily precipitation (Stuart and Isaac 1994). Du et al. (2013) compared TPI and Pearson correlation coefficients between precipitation and temperature in Northeast China, obtaining similar results using both methods. A similar exercise was conducted by Chrová and Holtanová (2018) for the European continent. The TPI index is a simple method used to characterize the relationship between temperature and precipitation, but it provides little information on the behavior of this relationship in the case of extreme values. The objective of the IR_t is to describe the positive or negative character of the temperature-precipitation relationship and quantify this relationship and the contribution to it of cold and warm days. The IR_t index, whose definition is based on the distribution functions of cold and warm days, and developed using half of the data (lower and upper quartiles of temperature) as the TPI index (based on the median), but the resulting information is very similar (Rodrigo 2022).

The aforementioned study tested the application of this index to four representative meteorological stations of the Iberian Peninsula (IP). The main objective of the present work is to extend the calculation of this index to a broader set of meteorological stations over a sufficiently long period to analyze changes in both the spatial and temporal distribution of the index. To this end, a total of 35 IP weather stations are used, with data corresponding to the period 1951–2019. Given its geographical location in the mid-latitudes, under the influence of the Atlantic Ocean and the Mediterranean Sea, and with marked orographic contrasts, the IP is a particularly interesting region for climate variability studies. Moreover, it has been cataloged as a 'hot spot' area for climate change (Giorgi 2008). The previously mentioned work also analyzed the modulating role of atmospheric circulation on the temperature-precipitation relationship by studying the influence of some teleconnection mechanisms, such as the East Atlantic (EA) pattern, the North Atlantic Oscillation (NAO), and the Western Mediterranean Oscillation (WeMO). The present work expands the set of possible predictors by adding the Eastern Atlantic/Western Russia (EA/WR) and Scandinavian (SCAN) patterns. The database and methodological basis of the study are described in Sect. 2. Section 3 analyzes and discusses the results obtained, and finally, some conclusions and future lines of work are presented.

2 Data and methods

2.1 Data

The database used in this study comprises daily rainfall amounts and daily mean temperatures from 35 locations covering the main climate domains of the IP during the period 1951–2019. The data sets were obtained from the European Climate Assessment & Dataset Project (ECA&D, Klein-Tank et al. 2002, data and metadata are available at <http://www.ecad.eu>). This database contains 220 Spanish and 39 Portuguese stations. In order to consider the largest possible number of stations with a long time record, series with data since 1951 were considered. The seasons of the year were defined in the usual way: winter (December, January, February), spring (March, April, May), summer (June, July, August) and fall (September, October, November). The time series of a station and a particular season was rejected if it had more than 9 days (about 10%) with data gaps. For each station time series of a season of the year was removed if it had more than six data gaps (about 10%). Data gaps were not filled (one of the objectives of this work is to find out the applicability of the index to different stations, and we preferred to use the most complete data series). As our interest resides in the covariability of rainfall and temperature, these restrictions were applied simultaneously to both variables, reducing the number of stations selected to 35 (unfortunately, only two Portuguese stations survived in this exercise). Figure 1 shows the location of the selected stations, and Table 1 shows their principal geographical data. The selected set of stations is representative of the different climatic regimes in the IP, including stations located on the north coast, the Mediterranean coast, and central, southern and western areas (Martín Vide and Olcina 2001).



Fig. 1 Map with the 35 stations selected in the Iberian Peninsula (numerical code in Table 1 is included)

Table 1 Meteorological stations studied in this work (data from 1951–2019)

Code	Station	Latitude	Longitude	Height (m asl)	Gaps (days, %)
1	A Coruña	43°22'N	08°23'W	21	0.00
2	Albacete	38°59'N	01°51'W	681	0.20
3	Alicante	38°20'N	00°28'W	5	0.04
4	Almería	36°50'N	2°27'W	16	0.10
5	Barcelona	41°22'N	02°10'E	13	0.30
6	Bilbao	43°15'N	02°57'W	6	0.90
7	Braganza	41°48'N	06°45'W	700	1.40
8	Burgos	42°20'N	03°41'W	859	0.07
9	Cáceres	39°28'N	06°22'W	457	0.00
10	Castellón	39°58'N	00°03'W	27	0.70
11	Ciudad Real	38°59'N	03°55'W	625	0.05
12	Gijón	43°32'N	05°42'W	3	0.07
13	Granada	37°10'N	03°36'W	684	0.70
14	Huelva	37°15'N	06°57'W	24	0.30
15	Huesca	42°08'N	00°24'W	483	2.00
16	León	42°35'N	05°34'W	837	0.20
17	Lisboa	38°43'N	09°10'W	2	5.00
18	Lleida	41°37'N	00°38'E	167	0.01
19	Logroño	42°28'N	02°26'W	384	0.02
20	Madrid	40°25'N	03°41'W	657	0.00
21	Málaga	36°43'N	04°25'W	8	0.40
22	Murcia	37°59'N	01°07'W	42	0.80
23	Ponferrada	42°32'N	06°35'W	512	0.10
24	Salamanca	40°57'N	05°39'W	798	0.05
25	San Sebastián	43°19'N	01°59'W	7	0.05
26	Santander	43°28'N	03°48'W	8	0.05
27	Santiago	42°53'N	08°32'W	260	0.20
28	Sevilla	37°23'N	05°59'W	11	0.30
29	Soria	41°46'N	02°28'W	1061	0.30
30	Tortosa	40°48'N	00°31'E	14	0.00
31	Valencia	39°28'N	00°22'W	16	0.30
32	Valladolid	41°39'N	04°43'W	690	0.20
33	Vitoria	42°50'N	02°40'W	539	1.10
34	Zamora	41°29'N	05°45'W	649	1.30
35	Zaragoza	41°39'N	00°53'W	208	0.02

Monthly data from the EA, EA/WR, NAO, and SCAN patterns, available from Climate Prediction Center (<http://www.nvcp.noaa.gov/teledoc>), as well as from the WeMO (available at <http://cru.uea.uk>) were also used. The monthly data were averaged to obtain a seasonal index in each case.

2.2 Methods

We define a day, i , as warm (cold) if its mean temperature is $T_i > T_{75}$ ($T_i < T_{25}$), where T_{25} and T_{75} are the 25th and 75th percentiles of the daily mean temperature corresponding to the reference period 1971–2000. This reference period was chosen because it is the central 30-year period within the entire dataset of the 1951–2019 period and thus avoiding the possible bias

that global warming in the last decades of the twentieth century and the beginning of the twenty-first century would introduce in the results. For each year t , the IR_t index is defined as the difference between the percentage of rainfall corresponding to warm days and that corresponding to cold days, that is,

$$IR_t = 100 \left[\frac{\sum_i \theta_w(T_i) R_i}{\sum_i R_i} - \frac{\sum_i \theta_c(T_i) R_i}{\sum_i R_i} \right] \quad (1)$$

where

$$\theta_c(T_i) = \begin{cases} 1 & \text{if } T_i < T_{25} \\ 0 & \text{if } T_i \geq T_{25} \end{cases} \text{ and } \theta_w(T_i) = \begin{cases} 1 & \text{if } T_i > T_{75} \\ 0 & \text{if } T_i \leq T_{75} \end{cases} \quad (2)$$

R_i is the daily rainfall for each day i of year t . The index was calculated at the seasonal level for each of the 35 weather stations and each year t . The units of the index are percentages. If $IR_t > 0$ ($IR_t < 0$), there is a predominance of precipitation on warm (cold) days of year t , and consequently, the relationship between precipitation and temperature is positive (negative).

Cluster analysis was used to synthesize the information and search for regionalization of the IR_t index. Cluster analysis is an effective statistical method for grouping stations into climatologically homogeneous regions (Joliffe and Philipp 2010; Mahlstein and Knutti 2010) and is widely used in climatological research. Thus, we can find examples in the identification of climatic zones from places as disparate as Italy (Calmanti et al. 2015), Brazil (Teodoro et al. 2016), the Balkan peninsula (Nojarov 2017), Bangladesh (Siraj-Ud-Doula 2019), or Borneo (Sa'adi et al. 2021), the spatial distribution of drought indices in Iran (Zolfaghari et al. 2019), or Pakistan (Ullah et al. 2020), or spatial rainfall patterns in Algeria (Zerouali et al. 2022). Ward's minimum variance method (Ward 1963) was applied in this study to cluster the IR_t index data. This method, with Euclidean distance as the similarity measure, is one of the most frequently used (Falquina and Gallardo 2017). There are examples in the Iberian Peninsula of its use in the regionalization of seasonal rainfall (Muñoz-Díaz and Rodrigo 2004) or the spatial distribution of extreme temperature indices (Fernández-Montes and Rodrigo 2012). A significant practical problem is choosing the appropriate number of clusters to represent the data set, although there are no universally accepted objective techniques to achieve this goal. A common approach is to inspect a plot of the distances between clusters as a function of the stages in the aggregation process. When similar clusters are grouped together in the early stages, the distances are small and gradually increase from one step to the next. At the end of the process, there may be only a few clusters separated by large distances. If a point can be discerned at which the distances increase considerably, then the clustering process can be stopped just before that step. Inspection of the distance plot and the tree diagram, or dendrogram, where the successive clustering steps are summarized, provides the number of clusters and the members of each cluster (Wilks 2019).

Once the main clusters into which the data can be grouped for each season of the year were determined, the cluster index was obtained as the average of the IR_t indices of the cluster members, that is,

$$\langle IR \rangle = \frac{1}{K} \sum_{j=1}^K IR_{tj} \quad (3)$$

where K is the number of elements in the cluster, and IR_{tj} is the index value of year t for element j . This step allows

us to discern each cluster's main characteristics of the index behavior.

The next step was to analyze the time series of the $\langle IR \rangle$ index. For this purpose, the Mann–Kendall test was applied to detect any significant trend. The analysis also used the sum of anomalies (value of the index for each year t minus the average of the entire period 1951–2019), accumulated over time (S_t), starting from the first to the last year of the series. An advantage of cumulative anomalies is that they facilitate the detection of periods of predominant negative or positive anomalies: in case of the predominance of negative anomalies, the anomaly curve as a function of time is decreasing, while it is increasing in case of phases with the predominance of positive anomalies (Philipp et al. 2007). This method allows distinguishing between different sub-periods within the whole period; a minimum or a maximum in the cumulative anomaly curve indicates a point of change in the behavior of the series. The subperiods obtained can then be compared using statistics such as the t -test for the difference between the means (all statistical tests were evaluated at the 95% confidence level).

Trends in precipitation are strongly modulated in our area of interest by large-scale atmospheric circulation (Zappa 2019). The analysis focused on teleconnection indices that primarily affect IP (López-Bustins et al. 2008; González Reviriego et al. 2014; Ríos-Cornejo et al. 2015; Merino et al. 2018): EA, NAO, EA/WR, and SCAN. The influence of the teleconnection indexes on the $\langle IR \rangle$ indexes was calculated by multiple regression analysis. As these teleconnection indices were obtained from a principal component analysis of the SLP field (Barnston and Livezey 1987), their orthogonality avoids the potential problem of multicollinearity among the predictors of the regression analysis. In addition, the index corresponding to WeMO was added, given the importance of this index for IP and that it did not show significant correlations with the rest of the indexes (Martín-Vide and López-Bustins 2006). The general model can then be written as

$$\langle IR \rangle = a_0 + \sum_k a_k P_{kt} + \varepsilon_t \quad (4)$$

where a_0 is the regression constant, a_k is the coefficient of the teleconnection index P_k , P_{kt} is the value of the index of pattern k in year t , and ε_t is the residuals of the regression. The stepwise regression method was applied to investigate the relative importance of the predictors, using the 0.05 significance level as a condition for the entry of a new predictor in the models. The adjusted R^2 statistic was calculated to estimate the percentage of variance explained by the model. Finally, the residuals were inspected to evaluate the reliability of the models, checking whether they met the condition of random, Gaussian, and null mean series.

The Kolmogorov–Smirnov test ($K-S_{res}$) with Lilliefors correction was applied to estimate normality, the confidence interval of the mean of the residuals (CI_{res}) was calculated at the 95% confidence level to test the mean null hypothesis (we accepted the mean null hypothesis if $0 \in CI_{res}$), and the Durbin-Watson (DW) statistic to determine if there was significant autocorrelation in the residuals. Since DW is approximately equal to $2(1 - r)$, where r is the first-order autocorrelation coefficient of the residuals, $DW = 2$ indicates that there is no autocorrelation (von Storch and Zwiers 1999). Considering that the maximum number of predictors is 5 and the size of each sample is 69 data, we can accept that there is no autocorrelation in the residuals if $DW \geq 1.4$ (Wilks 2019). If the alternative hypothesis is that errors are negatively correlated, then the statistic should be $4-DW$. The critical values consist of pairs DW_L and DW_U (see Tables II and III in Savin and White 1977) such as the null hypothesis can always be rejected if $\max(DW, 4-DW) < DW_L$ and

it should not be rejected if $\min(DW, 4-DW) > DW_U$ (von Storch and Zwiers 1999).

3 Results and discussion

3.1 Regionalization

Figure 2 shows the results of the application of cluster analysis to the winter indices. Visual inspection of the distance plots as a function of the grouping step (Fig. 2a) and the dendrogram (Fig. 2b) allows us to distinguish four clusters (Fig. 2c), which, depending on the geographic location of most of the stations of each cluster, are called Central-Northwest (CNW, stations indicated by blue color), Central-Northeast (CNE, green), East (E, red) and South (S, yellow). A similar regionalization was obtained by applying the non-hierarchical cluster K-means method to the correlation coefficients between temperatures and precipitation,

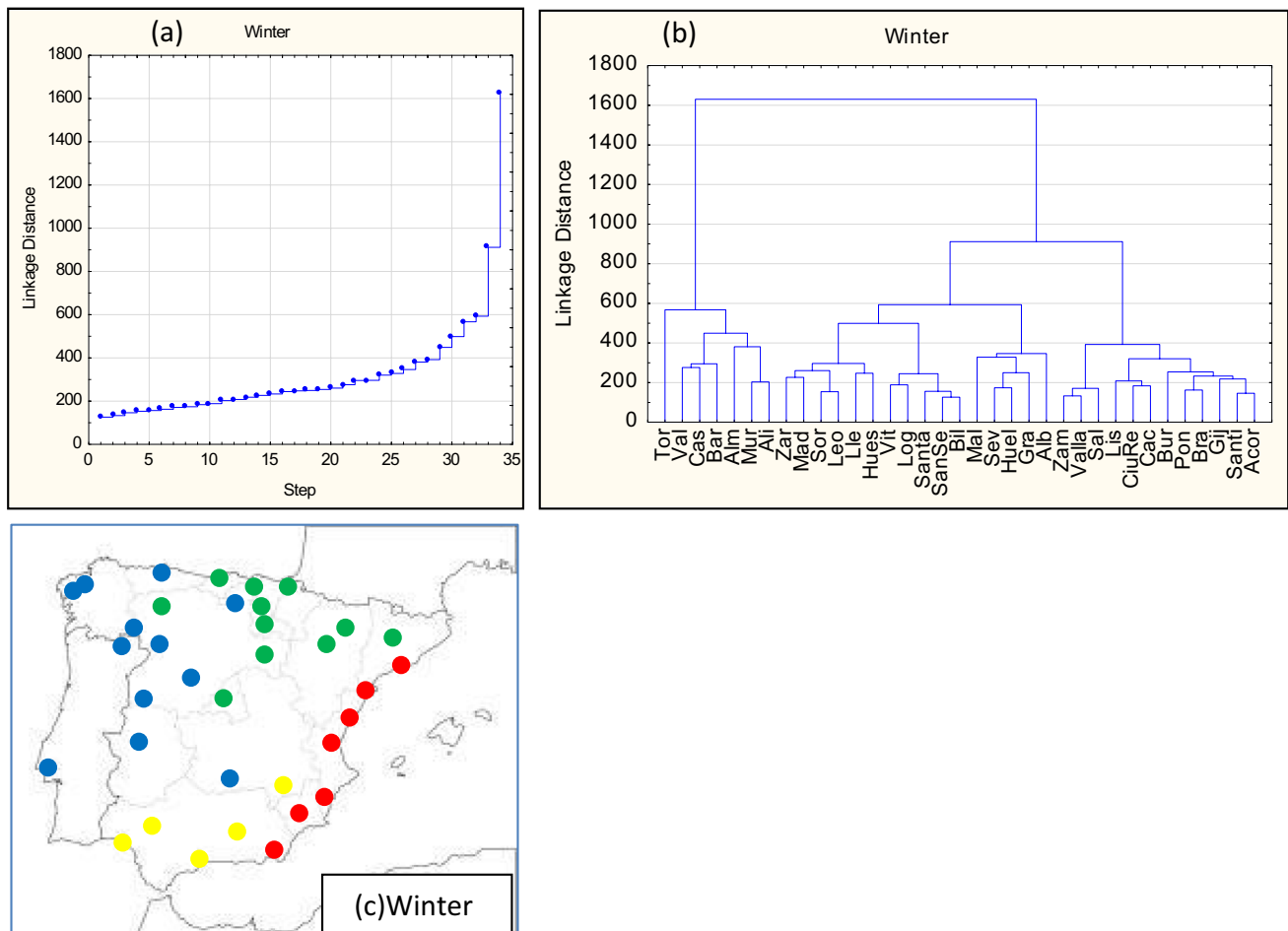


Fig. 2 Cluster analysis (euclidean distance, Ward's method) of the 35 stations for winter, 1951–2019. **a** Plot of linkage distance across steps; **b** Tree diagram for 35 variables. **c** Clusters: CNW (blue), CNE (Green), E (red), and S (yellow)

using regional model simulations for the last millennium (Fernández-Montes et al. 2017). In that work three regions were identified, a western region, which correlates with our CNW region; a region on the Mediterranean coast (our E region); and a transition region between them, which correlates with our CNE and S clusters. According to our dendrogram (Fig. 2b), these show less distance between them than with the other two clusters. Table 2 shows each cluster's basic statistics of the $\langle IR_t \rangle$ indices. Of note is the positive value of the mean value of the CNW index, whose 95% confidence interval (CI) has also shifted toward positive values, as opposed to the negative values for Cluster E, and values ≈ 0 for Clusters S and CNE. Fernández-Montes et al. (2017) find a positive correlation between temperatures and precipitation in the western area of the IP, motivated by a higher frequency of warm-wet and/or cold-dry winters, as well as a higher prevalence of negative relationships (warm-dry or cold-wet winters) in region E, and intermediate conditions in its transition region. In mid-latitude winters, low temperatures lead to early saturation, limiting the amount of precipitation and thus favoring the combination of cold-dry conditions. On the other hand, precipitation is mainly related to the advection of relatively warm and humid air from extratropical cyclones from the Atlantic, favoring warm-humid conditions. All this leads to a positive correlation between temperatures and precipitation (Trenberth and Shea 2005; Adler et al. 2008) and to a positive value of our $\langle IR \rangle$ index. As for the E region, with negative mean values for the index, the predominance of the W and NW circulation leads to warm-dry conditions due to its location in a rain shadow area (Föhn effect). Although the normality hypothesis cannot be rejected in any of the series (Kolmogorov–Smirnov statistic, median \approx mean), all index series present high variability, as

indicated by the standard deviation values (s in Table 2) and the range of index values. This result is also analogous to Fernández-Montes et al. (2017), who detected large fluctuations over time in their correlations.

The regionalization in spring (Fig. 3) allows us to distinguish four areas that show slight modifications compared to winter: Central-Northwest (CNW, stations in blue in Fig. 3c), East (E, red), Southwest (SW, yellow) and the one we have called Interior-North (IN, green). Only two stations (San Sebastian to the N of the IP) and Barcelona (to the NE) present apparently anomalous behavior, being grouped with the stations of the SW cluster. The fact that both are coastal stations, and the possible influence of local factors, could explain this result. In spring, all indices are clearly negative, except in the IN case, where the CI is slightly shifted towards positive index values. Again our regionalization is analogous to that of Fernández-Montes et al. (2017). Spring is a transition period between winter and summer. Thus, although the spatial distribution of the index follows the characteristics of winter, there is a growing tendency toward reinforcing the negative conditions typical of summer.

In summer (Fig. 4), our cluster analysis allows us to distinguish two regions, which we have called North (N, corresponding to the stations of the northern third of the IP, represented in blue color in Fig. 4c) and South (S, red color in Fig. 4c). The index values are clearly negative, particularly in the S area. The interpretation of the summer results is less conclusive, given the low rainfall in the IP during this time of year. In summer, moisture availability is the limiting factor for precipitation (Berg et al. 2009). Dry conditions are related to higher solar radiation and lower evaporative cooling, while humid summers are cooler due to, among other reasons, cloudiness, preventing radiative input (Berg et al.

Table 2 Main statistics of the index $\langle IR \rangle$ for the four seasons and clusters during the period 1951–2019

Season	Cluster	Mean(%)	CI(%)	Median(%)	s(%)	Range(%)	K-S value
Winter	CNW	+16	[+11;+22]	+15	22	[-30;+65]	0.07690
	CNE	-5	[-10;-1]	-4	20	[-50;+33]	0.06670
	E	-26	[-32;-20]	-23	24	[-75;+36]	0.05988
	S	+3	[-4;+10]	+3	28	[-64;+64]	0.07137
Spring	IN	-2	[-7;+3]	-1	21	[-54;+41]	0.07596
	E	-22	[-29;-15]	-26	28	[-68;+48]	0.09345
	SW	-37	[-42;-32]	-36	20	[-79;+28]	0.08195
Summer	CNW	-18	[-23;-14]	-18	19	[-54;+44]	0.07076
	N	-19	[-25;-12]	-21	26	[-79;+26]	0.06330
	S	-40	[-47;-33]	-45	28	[-83;+34]	0.09610
Fall	IN	-3	[-7;0]	-3	16	[-39;+34]	0.04584
	SE	-20	[-23;-16]	-19	15	[-61;+5]	0.07295
	NW	-25	[-24;-21]	-24	15	[-32;+8]	0.08732

CI=confidence interval for mean at the 95% level; s=standard deviation; K-S=Kolmogorov Smirnov statistic with Lilliefors correction (critical value for null hypothesis of normality at the 95% confidence level=0.10666)

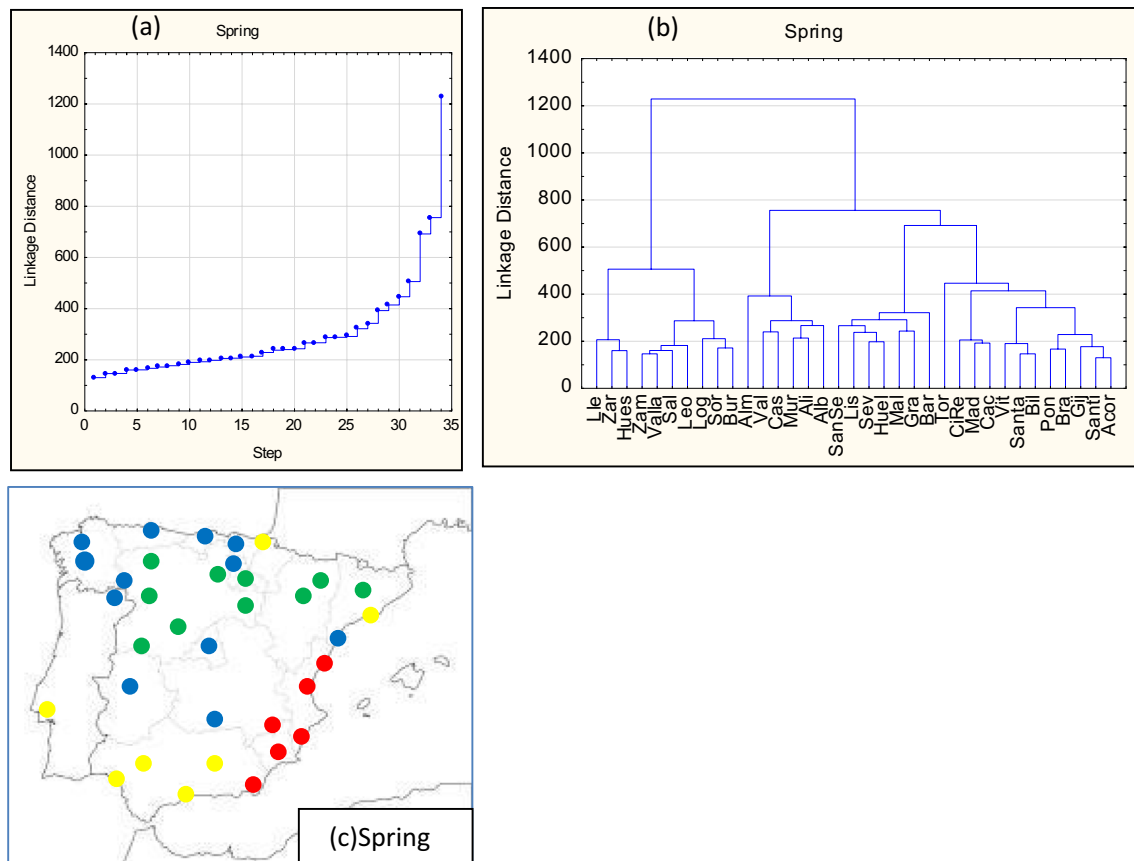


Fig. 3 Cluster analysis (euclidean distance, Ward's method) of the 35 stations for spring, 1951–2019. **(a)** Plot of linkage distance across steps; **(b)** Tree diagram for 35 variables. **(c)** Clusters: CNW (blue), IN (Green); E (red), and SW (yellow)

2015). All this leads to negative index values. The separation between the N and S clusters may be because precipitation in the North is more related to the advection of Atlantic cyclones, while in the S, it is due to the occurrence of convective storms (Fernández-Montes et al. 2017).

Figure 5 shows the results for the fall. In this instance, three clusters have been detected, named Northwest (NW, blue stations in Fig. 5c), Interior-North (IN, green) and Southeast (SE, red). Only one station to the NW of the IP, A Coruña, seems to show an anomalous behavior, being grouped with the Southeast stations. The possible influence of local factors (more important in fall) could explain this result, but this is an aspect that needs explanation. Fall, as a transition season between summer and winter, may present similar characteristics to summer (such as convective storms, especially in the SE area) and to winter (advection of Atlantic squalls to the NW of the IP), with the IN area remaining as a transition zone between both regions. There is some similarity with the regionalization of Fernández-Montes et al. (2017), who also detect a western region (NW, in our case), a region to the SE and an area that can be identified with our IN region. However, they distinguish a SW region

that is not detected here. This discrepancy may be due to the inadequacy of our database, with a minimal number of stations in southern Portugal.

These results indicate the strong seasonality of our index in the IP, with a spatial distribution that changes throughout the year, albeit showing a certain annual cycle, with winter and summer clearly differentiated and spring and fall as transition seasons between one and the other, show intermediate characteristics between the two. The negative value of the indices (except in the winter CNW region) reflects the expected behavior in the temperature-precipitation relationship of mid-latitude continental areas, which allows us to be confident in the suitability of our index for the study of the covariability of both variables.

3.2 Time series

Table 3 and Figs. 6, 7, 8 and 9 summarize the time series behavior of each cluster's <IR> indices for the year's four seasons. In the case of winter (Fig. 6), the Mann–Kendall test reports a slightly significant increasing trend in the

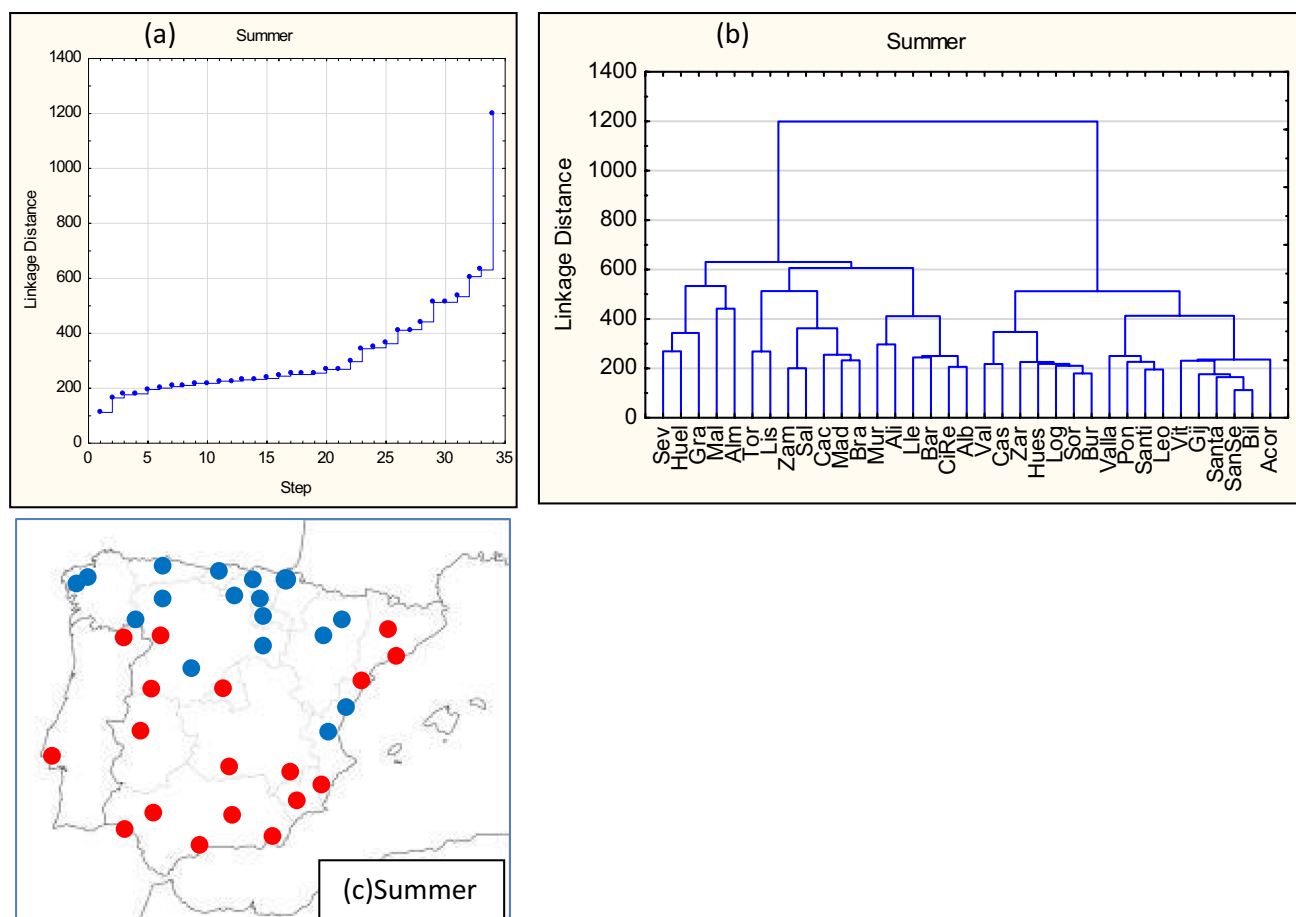


Fig. 4 Cluster analysis (euclidean distance, Ward's method) of the 35 stations for summer, 1951–2019. **(a)** Plot of linkage distance across steps; **(b)** Tree diagram for 35 variables. **(c)** Clusters: N (blue), and S (red)

CNW and CNE clusters, while the E and S clusters show no significant trend. The cumulative sum of deviations allows us to detect a minimum that would indicate a turning point in 1977 for the CNW cluster (Fig. 6b) and 1978 for the CNE cluster (Fig. 6d). In cluster S (Fig. 6f), on the other hand, there is no clear extreme value to establish a point of change, while in cluster E (Fig. 6h), the possible point of change would be located in 1986. The application of the t-test for differences between means between the two resulting subperiods shows significant differences between the mean values of the first and second subperiods for the CNW, CNE and E clusters, with a shift towards more positive (CNW cluster) or less negative (CNE and E clusters) values. These results would indicate a shift towards warm-humid (or, alternatively, cold-dry) conditions.

In spring (Fig. 7), significant increasing trends are found only in the SW and CNW clusters (Table 3), with the change point located in 1987. As in winter, the differences between the mean values of the resulting subperiods indicate a trend towards less negative values of the index, i.e., a shift from warm-dry (cold-wet) to warm-wet (cold-dry)

conditions, with differences that are significant for the four clusters detected. These increasing and significant trends are also detected in the summer clusters (Fig. 8), with change points in 1993 for cluster N and 1988 for Cluster S (Table 3). Once more, the trending behavior is for less negative values of the index, even more markedly than in spring, as indicated by the value of the t-test statistic of the difference between the means. Finally, in the fall (Fig. 9), an increasing and significant trend is only detected in the SE cluster, with a turning point in 1985 towards less negative index values.

The results presented in Table 3 and Figs. 6, 7, 8 and 9 show behavior of increasing evolution of the index, towards positive values in the CNW cluster in winter and IN in spring or towards less negative values in the rest of the clusters for each season of the year. This behavior indicates a general shift from warm-dry (cold-humid) to warm-humid (cold-dry) conditions. Although this trend has not yet culminated during the study period, it shows the same behavior already detected in the studies mentioned in the introduction on Europe (Blöschl et al. 2020) and China (Yang et al.

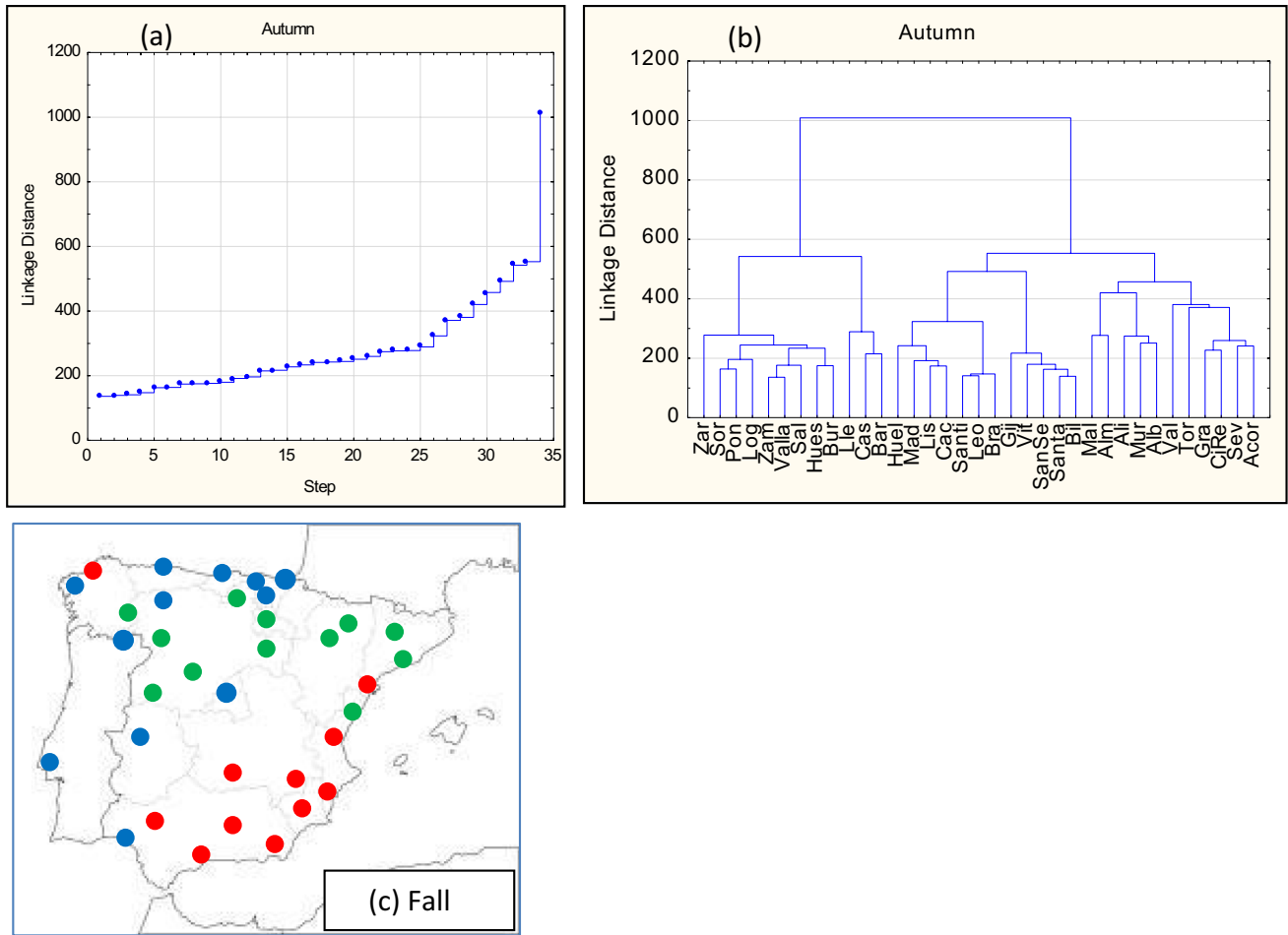


Fig. 5 Cluster analysis (euclidean distance, Ward’s method) of the 35 stations for fall, 1951–2019. (a) Plot of linkage distance across steps; (b) Tree diagram for 35 variables. (c) Clusters: NW (blue), IN (Green), and SE (red)

Table 3 Time evolution of the index $\langle IR \rangle$ for each cluster and season, 1951–2019

Season	Cluster	Mann–Kendall	Change point	$\langle IR \rangle$ (I)	$\langle IR \rangle$ (II)	t-test
Winter	CNW	+2.57*	1977	+6	+23	3.3*
	CNE	+2.62*	1978	-14	0	3.0*
	E	+1.90	1986	-33	-19	2.5*
	S	+1.09				
Spring	IN	+1.35	1986	-9	+6	3.17*
	E	+1.48	1978	-31	-16	2.27*
	SW	+2.78*	1987	-45	-28	3.81*
	CNW	+2.17*	1987	-26	-9	4.14*
Summer	N	+3.69*	1993	-30	0	5.5*
	S	+4.52*	1988	-56	-21	6.6*
Fall	IN	+0.85	1985	-7	0	1.8
	SE	+2.96*	1985	-28	-11	5.6*
	NW	+1.22	1980	-30	-21	2.6*

* = statistically significant at the 95% confidence level. $\langle IR \rangle$ mean value of the subperiods I from 1951 to the change point, and II, from the change point to 2019

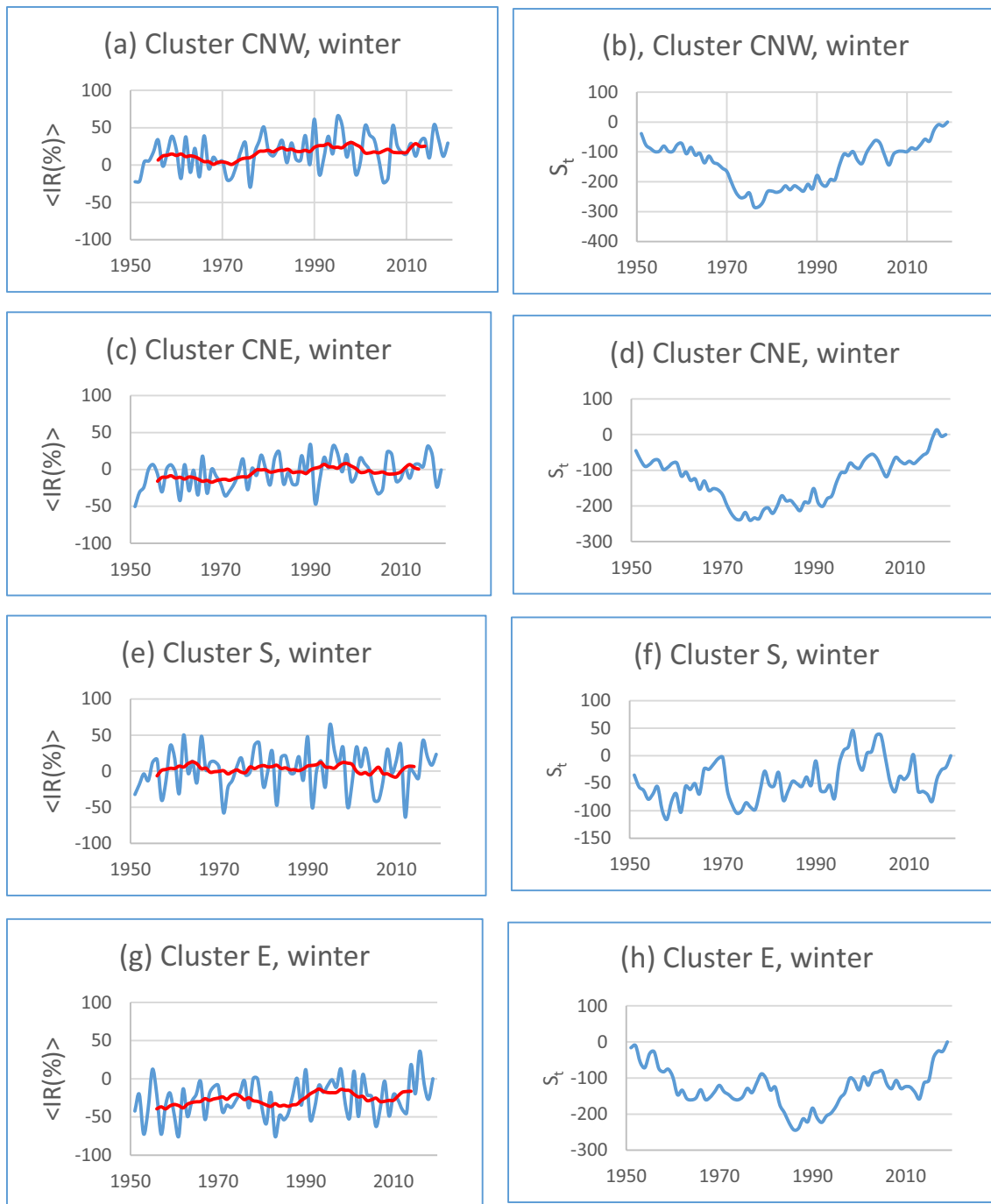


Fig. 6 Left: time series of the indices $\langle IR \rangle$ corresponding to winter clusters CNW (a), CNE (c), S(e), and E(g), for the period 1951–2019 (red line: 11 years moving averages). Right: Cumulative sum of devi-

ations corresponding to winter clusters CNW (b), CNE (d), S(f), and E(h), for the period 1951–2019

2021). Alexander et al. (2006), based on the analysis of the behavior of various indices of extreme values, also found a global change towards warmer and wetter conditions when comparing the periods 1951–1978 and 1979–2003.

The inflection point marking the changes found in our index is generally around the 1980s, with the earliest point

of change in 1977 (winter CNW cluster) and the latest in 1993 (summer N cluster). A similar periodization can be found in several studies analyzing the behavior of temperature extreme value indices (Hare and Mantua 2000; Alley et al. 2003; Alexander et al. 2006; Ivanov and Evtimov 2010; Ramos et al. 2014). Wu (2014) finds a change in

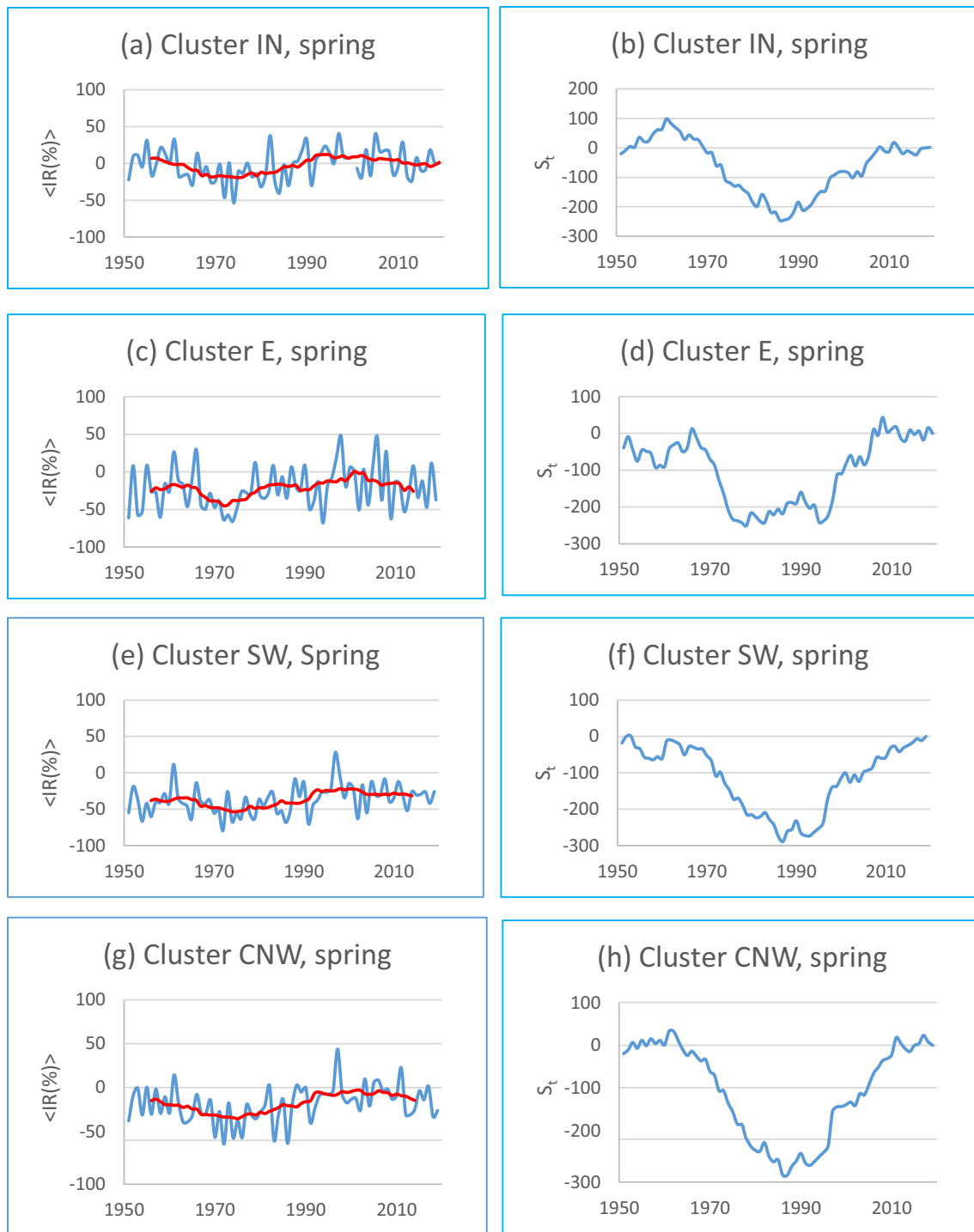


Fig. 7 Left: time series of the indices $\langle IR \rangle$ corresponding to spring clusters IN (a), E (c), SW (e), and CNW (g), for the period 1951–2019 (red line: 11 years moving averages). Right: cumulative sum of

deviations corresponding to spring clusters IN (b), E (d), SW (f), and CNW (h) for the period 1951–2019

temperature and precipitation covariability in East Asia precisely in the late 1970s. The weakening of the negative relationship between temperatures and precipitation could be explained as a consequence of the increase in

convective-type precipitation caused by the increase in temperatures (Rodrigo 2019), mainly in the summer S and fall SE clusters, which show the highest t-test values

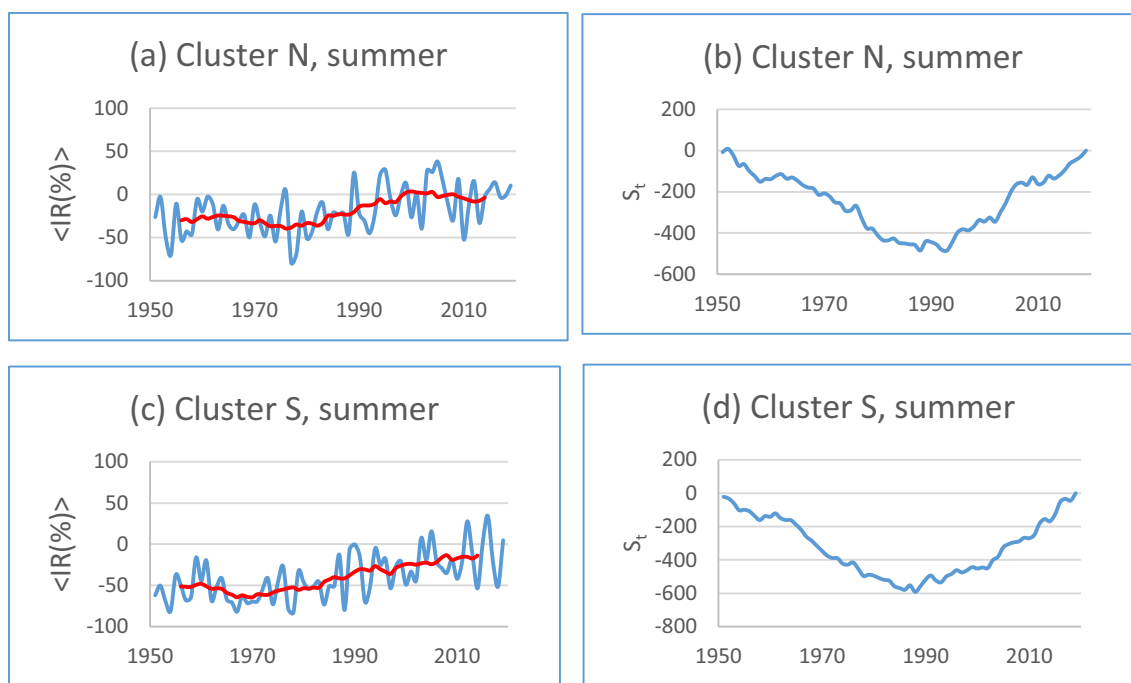


Fig. 8 Left: time series of the indices $\langle IR \rangle$ corresponding to summer clusters N (a), and S (c), for the period 1951–2019 (red line: 11 years moving averages). Right: Cumulative sum of deviations corresponding to summer clusters N (b), and S (d), for the period 1951–2019

(Table 3). However, this is an aspect that deserves further investigation.

3.3 Regression models

Atmospheric circulation can modify thermodynamic relationships between temperatures and precipitation, either intensifying or attenuating them (Berg et al. 2015). In our study, the regression models provide the dynamic component with the main teleconnection patterns affecting IP as predictors. The positive or negative phases of these patterns determine the predominance of anticyclonic or cyclonic conditions and the possibility of advections over the IP, either from the Atlantic and/or the Mediterranean, which modify the thermodynamic conditions. The models proposed are intended to assess the contribution of atmospheric dynamics to the $\langle IR \rangle$ indices. However, other physical mechanisms, particularly thermodynamic relationships between the two variables and soil-atmosphere feedback, are essential for understanding temperature-precipitation covariability (Trenberth 2022) and will be the subject of future work.

Table 4 summarizes the results of the regression models between the $\langle IR \rangle$ index values and the EA, EA/WR, NAO, SCAN, and WeMO teleconnection indices. The blanks correspond to variables not used in the final model. Only in one case (fall IN cluster) it was not possible to find a model that explained, at least in part, the variability of the $\langle IR \rangle$ index. Perhaps the predominance of local conditions at this time

of the year may explain this result. In this regard, several previous studies (El Kenawy et al. 2012; Ríos-Cornejo et al. 2015) find that correlations between mean IP temperatures and teleconnection patterns are weaker in the fall. In the remaining cases, the analysis of the residuals shows that they behave as normal series ($K-S < 0.10666$, critical value for the null hypothesis of normality), of the null mean ($0 \in CI(res)$), and without autocorrelation (DW values), which allows confidence in the reliability of the models. The R^2 coefficient indicates the percentage of variability of our dependent variable explained by the model. The highest values are around 40% in the CNW regions in winter and spring and CNE in winter, justifying atmospheric dynamics' modulating (or, if you will, secondary) role in the temperature-precipitation relationship.

The constant regression a_0 is the value of the index $\langle IR \rangle$ when all predictors are in their neutral phase ($P_k = 0, \forall k$). It can thus be interpreted as the thermodynamic component of the relationship between temperatures and precipitation. It can be seen that $a_0 < 0$ for all clusters and seasons except the CNW cluster in winter. Low winter temperatures in the northwestern area of the IP lead to early saturation, limiting the amount of precipitation and thus favoring the combination of cold-dry conditions and the positive value of the index (Trenberth and Shea 2005). Thus, the T_{75} value in stations such as León, Salamanca and Valladolid is 6.2, 6.8 and 6.3 °C, respectively. In the other regions, we find higher values for T_{75} . For example,

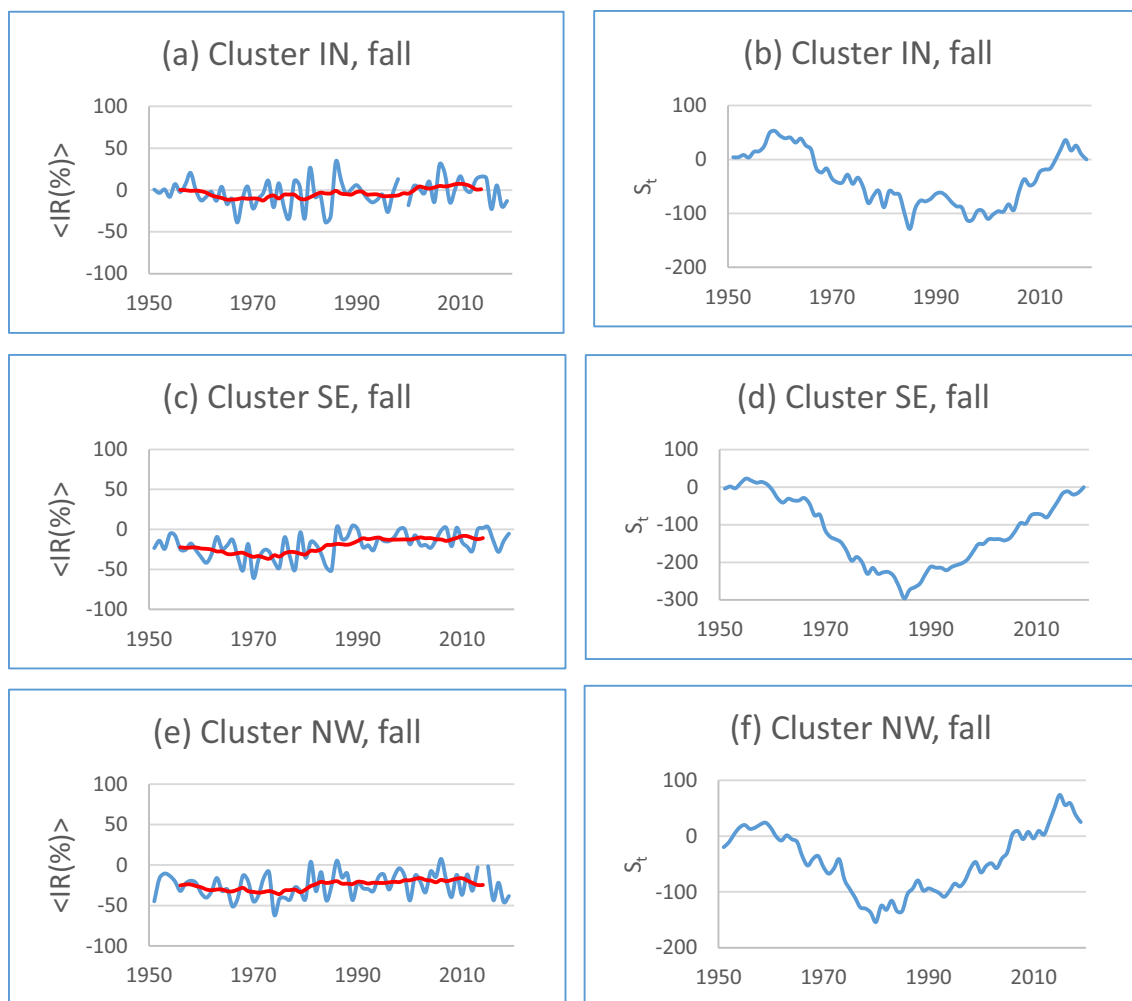


Fig. 9 Left: time series of the indices $\langle IR \rangle$ corresponding to fall clusters IN (a), SE (c), and NW (e), for the period 1951–2019 (red line: 11 years moving averages). Right: Cumulative sum of devia-

tions corresponding to fall clusters IN (b), SE (d), and NW (f) for the period 1951–2019

in region E (Mediterranean coast), it reaches values of 12.9 (Murcia), 13.6 (Alicante), or 14.3 °C (Barcelona). In the winter clusters that mark the transition between the two regions (CNE and S), the null value of a_0 would indicate the compensation between the different physical mechanisms that affect the relationship between temperatures and precipitation (the values of the T_{75} percentile in stations in this transition area are, in general terms, intermediate between the values of the other two clusters, thus, for example, in Madrid and Zaragoza, they are, respectively, 8.7 and 9.5 °C). For all other seasons, the negative sign of a_0 would therefore indicate the result that is to be expected in mid-latitude continental areas (Trenberth 2011; Adler et al. 2008; Cong and Brady 2012).

Figure 10 compares the observed values of the index and the values estimated from the linear model (left), as well as the residuals for each of the winter clusters (right). In winter,

a significant influence of the EA index was observed in all four clusters (Table 4). The EA pattern is characterized by a low pressure center located to the west of Ireland, approximately 55°N and 20–35°W (Hall and Hanna 2018), wherein the positive phase of the EA causes the advection of moist and relatively warm air masses from the south and southwest North Atlantic over the IP, leading to increased temperatures and precipitation. Numerous studies report a strong relationship between EA and temperature variations in the IP (see, for example, Ríos-Cornejo et al. 2015), which explains the value of the coefficient $a_{EA} > 0$, indicating that in the case of the CNW cluster, the positive relationship is intensified, while in the case of the E cluster, the negative relationship between temperatures and precipitation is weakened.

Another significant pattern is NAO, which affects the S cluster with $a_{NAO} < 0$. Indeed, the highest correlations between NAO and the SPEI drought index are found in the

Table 4 Multiple linear regression models between $\langle IR_t \rangle$ for each season and cluster and the teleconnection patterns EA, EA/WR, NAO, SCAN, and WeMO during the period 1951–2019 (only the coefficients \pm standard error significant at the 95% confidence level are indicated)

Season	Cluster	$a_0(\%)$	$a_{EA}(\%)$	$a_{EA/WR}(\%)$	$a_{NAO}(\%)$	$a_{SCAN}(\%)$	$a_{WeMO}(\%)$	R^2	e	CI_{res}	DW	$K-S_{res}$
Winter	CNW	$+22 \pm 2$	$+17 \pm 2$					0.42	17	[-5; +3]	2.01	0.05010
	CNE		$+14 \pm 2$			-7 ± 3		0.41	15	[-4; +4]	1.87	0.05677
	E	-23 ± 3	$+12 \pm 3$					0.18	22	[-5; +6]	2.00	0.09709
	S		$+14 \pm 3$		-12 ± 4			0.23	24	[-2; +10]	2.22	0.08719
Spring	IN					-14 ± 4	-7 ± 3	0.28	18	[-8; 0]	1.61	0.05341
	E	-21 ± 4	$+14 \pm 5$					0.09	27	[-4; +8]	2.04	0.07672
	SW	-38 ± 2	$+10 \pm 3$			-10 ± 4	-7 ± 3	0.31	17	[-3; +5]	1.57	0.09190
	CNW	-21 ± 2				-12 ± 3	-11 ± 2	0.42	14	[-4; +3]	1.48	0.05287
Summer	N	-18 ± 3					-12 ± 3	0.22	23	[-8; +3]	1.80	0.04251
	S	-39 ± 3					-12 ± 3	0.30	23	[-8; +3]	1.61	0.07471
Autumn	IN											
	SE	-20 ± 2					-5 ± 2	0.06	15	[-4; +3]	1.63	0.07149
	NW	-23 ± 2				-7 ± 3		0.14	14	[-4; +3]	1.97	0.06955

R^2 = adjusted R^2 coefficient; e = standard error of estimate; CI_{res} = confidence interval for mean of residuals at the 95% level; DW = Durbin-Watson statistic of residuals; $K-S_{res}$ = Kolmogorov–Smirnov statistic of residuals with Lilliefors correction (critical value for null hypothesis of normality at the 95% confidence level = 0.10666)

South of the IP (Manzano et al. 2019). The NAO is defined by a meridional dipole of sea level pressure between the Icelandic Low and the Azores Anticyclone (Hurrell et al. 2003). Its role in the variability of precipitation in the western sector of the IP is well known (see, for example, López-Bustins et al. 2008): the positive phase determines the predominance of anticyclonic conditions and low precipitation, while the negative phase is related to the advection of Atlantic squalls that increase precipitation, especially in winter. Given that $a_{NAO} < 0$, we obtain a negative contribution to the index value during the positive phase of the NAO. Under this phase, anticyclonic conditions determine low precipitation and higher maximum temperatures (Merino et al. 2018), leading to a negative relationship between temperatures and precipitation. In the negative phase of the NAO, on the other hand, with $a_{NAO} < 0$, we would obtain a positive contribution. The negative phase, with cyclonic conditions and overcast skies, is associated with higher precipitation and higher minimum temperatures (Trigo et al. 2002), thus resulting in a positive relationship. The fact that we are working with mean temperatures (and not with maxima and minima) may explain the lack of influence of this pattern in the rest of the clusters, where the effects of the NAO on the maximum and minimum temperatures would be compensated, especially in the CNW cluster. This result suggests an interest in studying our index using maximum and minimum temperatures instead of average temperatures, which will be the objective of future work. Finally, the influence of the SCAN pattern in the CNE cluster is also appreciated, with $a_{SCAN} < 0$. This pattern is characterized by a center of action over Scandinavia and weak centers of opposite signs over Western Europe and Eastern Russia. The positive phase of this pattern is

related to blocking anticyclones over Scandinavia and Russia and low pressure over the Iberian Peninsula, which leads to lower temperatures due to the advection of cold air from the NE, and higher precipitation, thus explaining why its effect is mainly detected in the CNE cluster. Thus, in the positive phase, since $a_{SCAN} < 0$, we would have a negative contribution to the behavior of the index. In the negative phase, the pattern is inverted, with a predominance of anticyclonic conditions over IP (El Kenawy et al. 2012), leading, in this case, to a positive relationship. As for the other two patterns, no influences of the EA/WR pattern and the winter WeMO pattern are detected. Regarding the EA/WR, Rust et al. (2015) found only weak signs of this pattern in monthly mean temperatures over Europe, explaining its absence in all models in Table 4.

Figure 11 summarizes the behavior of the spring models. In this case, the positive influence of the EA pattern in the E and SW clusters, as well as the negative influence of the SCAN pattern in the IN, SW and CNW clusters, is still evident. The appearance of the negative influence of the WeMO pattern in the IN, SW and CNW clusters is noteworthy. El Kenawy et al. (2012) also found that the main patterns affecting the mean temperature in the NE of the IP (corresponding to our IN cluster) are EA, SCAN and WeMO. Furthermore, Ríos-Cornejo et al. (2015) note that the area most influenced by EA in spring is the Mediterranean coast (our E cluster). The WeMO oscillation, in its positive phase, is characterized by a center of high pressure over northern Italy and low pressure to the SW of the IP, which causes the advection of NW air (relatively cold and humid). In contrast, in its negative phase, it would be the opposite situation, which would cause the advection of warm and humid air from

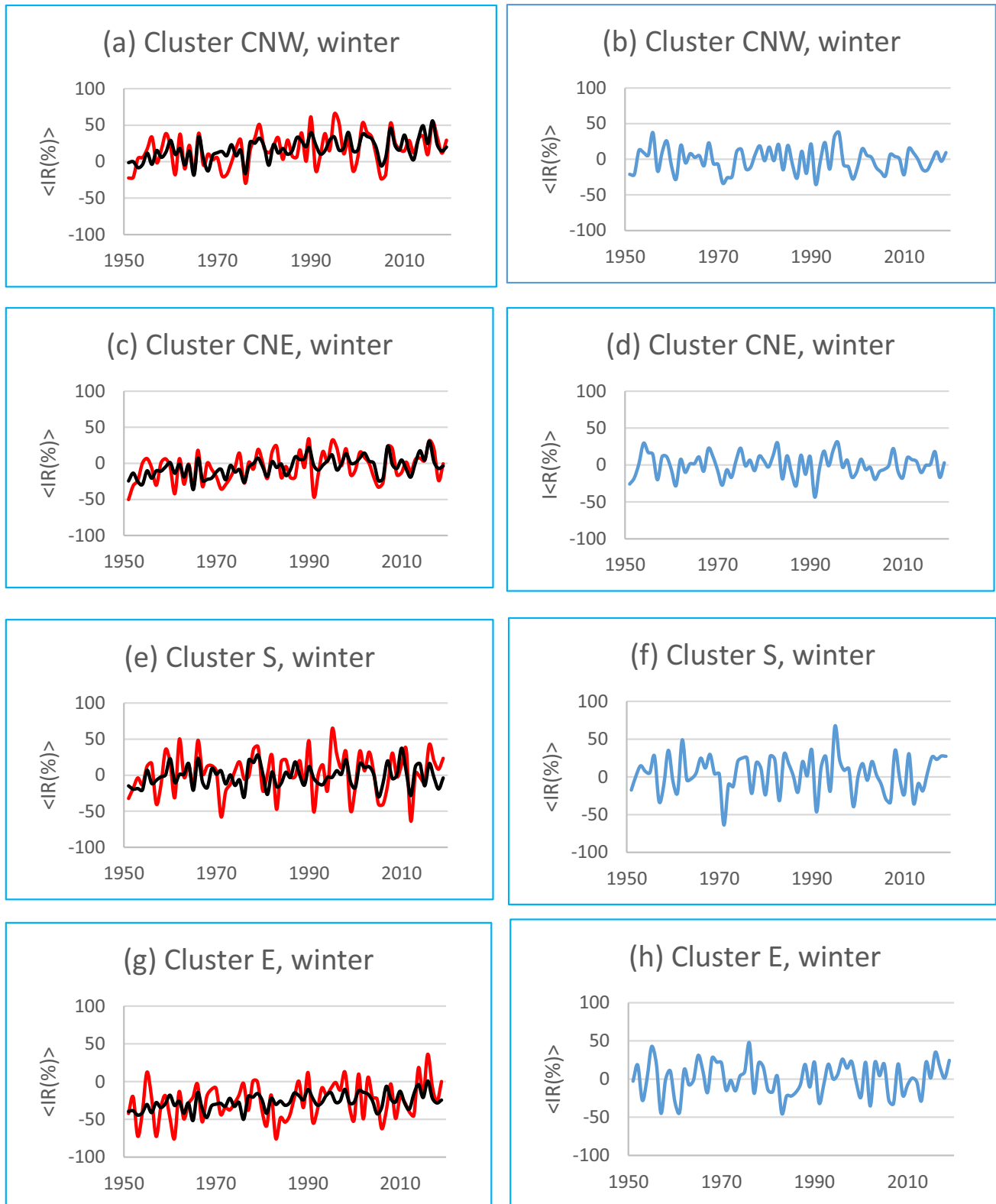


Fig. 10 Left: comparison between data (red line) and models (black line) for winter clusters CNW (a), CNE (c), S (e), and E (g) for the period 1951–2019. Right: Residuals of the models of the winter clusters CNW (b), CNE (d), S (f), and E (h) for the period 1951–2019

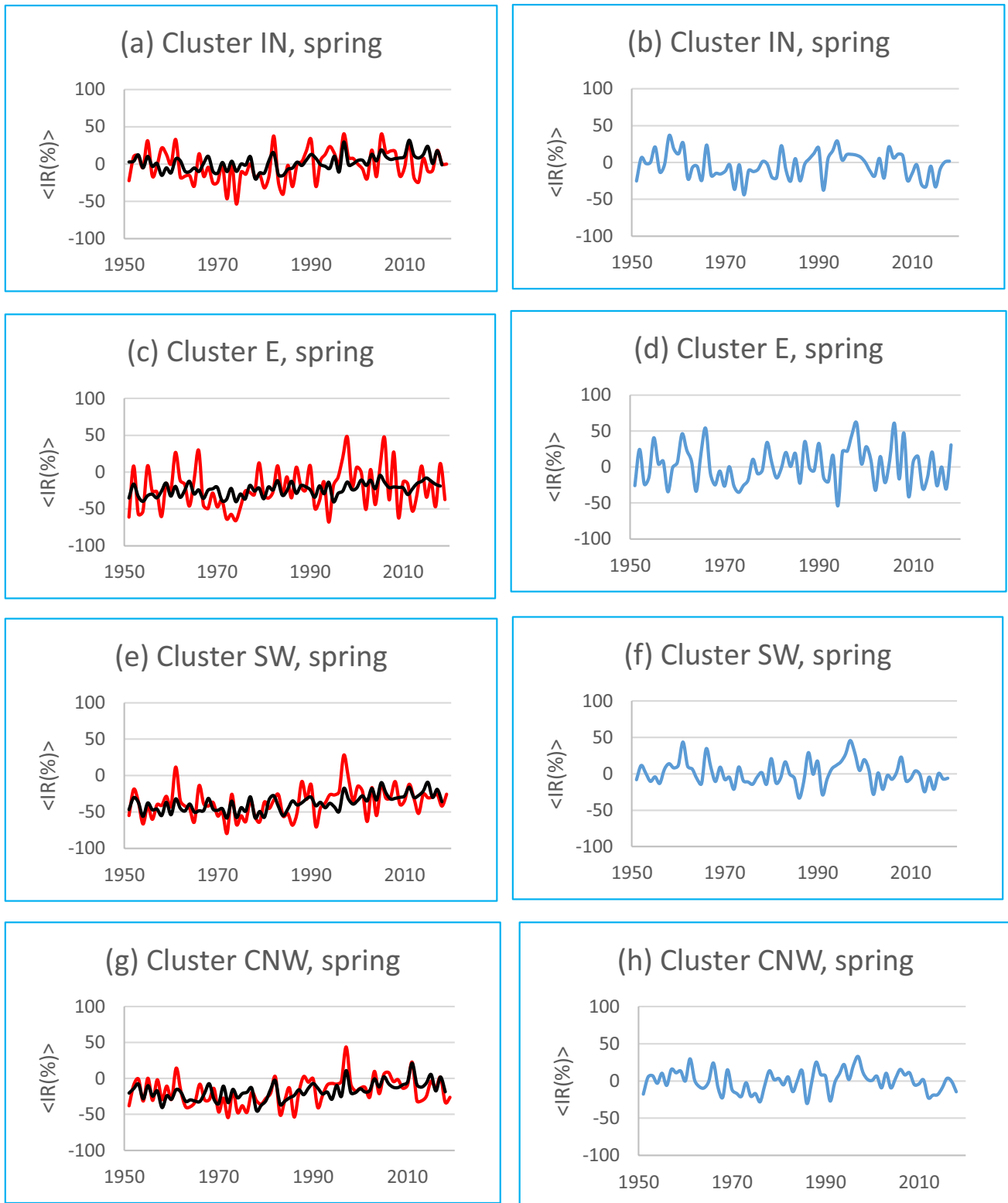


Fig. 11 Left: comparison between data (red line) and models (black line) for spring clusters IN (a), E (c), SW (e), and CNW (g) for the period 1951–2019. Right: residuals of the models of the spring clusters IN (b), E (d), SW (f), and CNW (h) for the period 1951–2019

the Mediterranean (Martín-Vide and López-Bustins 2006). Since $a_{\text{WeMO}} < 0$, the positive phase of the WeMO results in a negative contribution to the index, while the negative

phase would result in a positive contribution. The role of the WeMO in the summer is also noteworthy (Fig. 12) and in the fall SE cluster (Fig. 13). According to Ríos-Cornejo

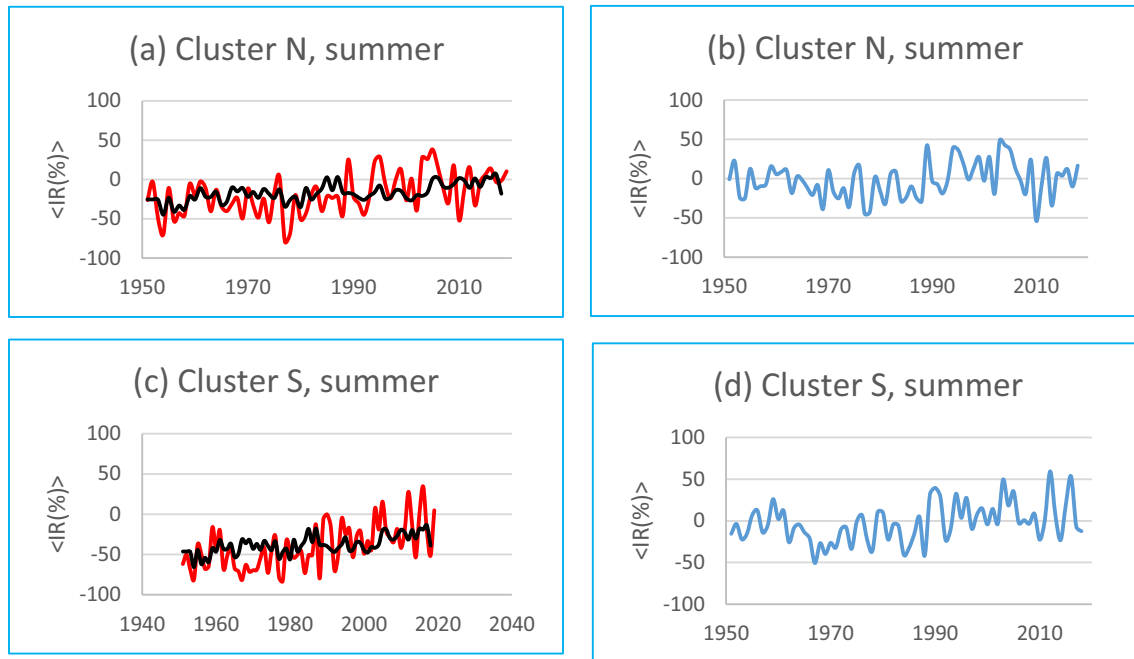


Fig. 12 Left: comparison between data (red line) and models (black line) for summer clusters N (a), and S (c) for the period 1951–2019. Right: Residuals of the models of summer clusters N (b), and S (d) for the period 1951–2019

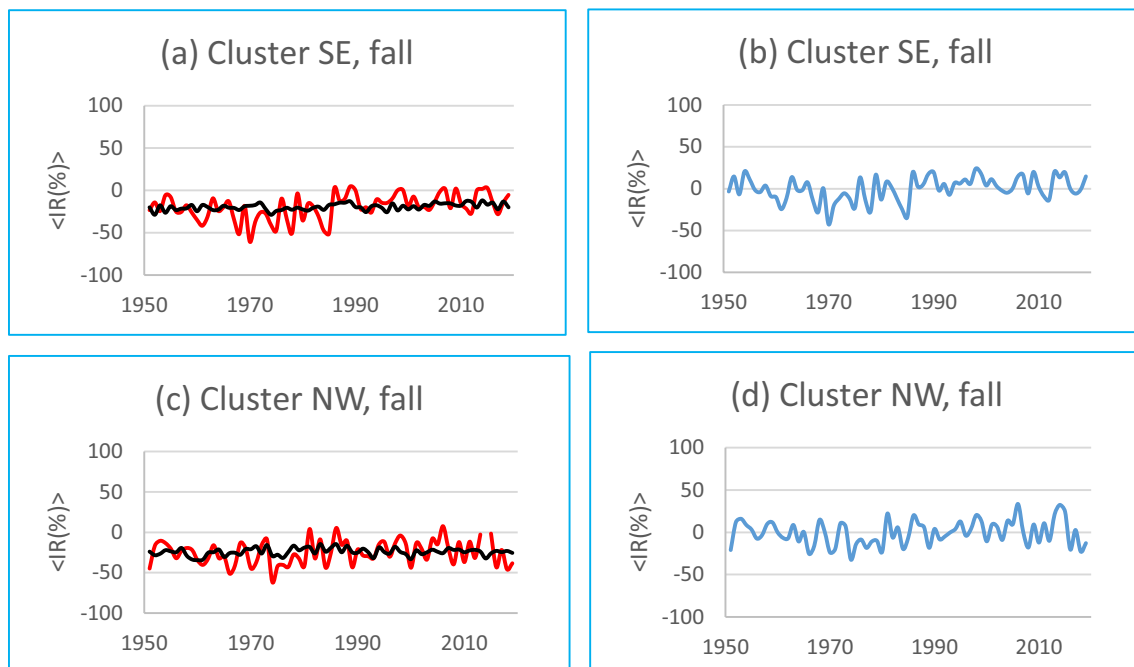


Fig. 13 Left: comparison between data (red line) and models (black line) for fall clusters SE (a), and NW (c) for the period 1951–2019. Right: Residuals of the models of fall clusters SE (b), and NW (d) for the period 1951–2019

Table 5 Mann–Kendall test of the time series of the teleconnection patterns EA, EA/WR, NAO, SCAN, and WeMO during the period 1951–2019

Pattern	Winter	Spring	Summer	Fall
EA	+4.37*	+4.04*	+5.66*	+4.74*
EA/WR	+0.17	-0.32	-3.44*	-2.56*
NAO	+3.79*	+2.78*	-1.51	-0.91
SCAN	-0.60	-1.80	-2.48*	-0.96
WeMO	-1.94	-4.41*	-5.02*	-0.32

* = trend statistically significant at the 95% confidence level

et al. (2015), the WeMO has a greater influence on the mean temperature of the warm months.

Given that the residuals of all models show Gaussian series behavior, zero mean and no autocorrelation (Table 4), we may wonder whether the trends detected in the behavior of the $\langle IR \rangle$ indices (Table 3) are related to the behavior of the teleconnection patterns. Table 5 summarizes the application of the Mann–Kendall test to search for trends in the teleconnection pattern indices for each season of the year. In winter, the EA and NAO patterns show an increasing trend toward positive index values, which could explain the significantly increasing trend of the $\langle IR \rangle$ index in the CNW and CNE clusters. In the case of cluster S, the positive trend of the EA ($a_{EA} > 0$) would be canceled by the negative contribution of the NAO ($a_{NAO} < 0$). As for cluster E, no significant trend was detected, but in this case, the dynamic influence, according to the R^2 coefficient, would be only 18% (Table 4). In spring, the SW and CNW cluster indices showed a significant increasing trend, which the increasing trend of EA could explain and the decreasing trend of WeMO ($a_{WeMO} < 0$). The increasing trends in the summer cluster indices can be explained by the contribution of the WeMO pattern, given its significant negative trend and a_{WeMO} value < 0 . Finally, in the fall, only the SE cluster showed a significant increasing trend that could not be explained by the teleconnection patterns (WeMO shows no significant trend in this season, and the R^2 coefficient indicates a minimal contribution to the variability, only 6%). One hypothesis to explain this behavior would be the increase in convective precipitation (Ruiz-Leo et al. 2013). Rising temperatures lead to greater vertical instability, more vigorous convection, and, therefore, an increase in convective precipitation. As a result, it would positively contribute to the IR_t index. In general terms, then, except for this last case, the trends found in the $\langle IR \rangle$ indices can be related to the behavior of the teleconnection patterns. The role of atmospheric dynamics, then, is to modulate the thermodynamic relationship between temperatures and precipitation, weakening or intensifying the positive or negative relationship between temperatures and precipitation and causing

a slight shift, with increasing trends in the cluster indices, from warm-dry (cold-humid) to warm-humid (cold-dry) conditions.

4 Conclusions

The main conclusions of this study can be summarized as follows:

- The IR_t index is a valuable tool for studying temperature-precipitation relationships in the IP.
- Strong seasonality of our index has been detected in the IP, with a spatial distribution that changes throughout the year but shows a certain annual cycle, with winter and summer clearly differentiated. In contrast, spring and fall, as transition seasons between one and the other, show intermediate characteristics between the two. In this sense, it could be interesting to use only two seasons, extended winter and summer.
- The results in Table 3 and Figs. 6, 7, 8 and 9 show the increasing evolution of the index toward positive values in the CNW cluster in winter and IN in spring. It also shows an evolution towards less negative values in the rest of the clusters for each season. This behavior indicates a weakening of the negative relationship between both variables, with a slight shift from warm-dry (cold-wet) conditions to warm-wet (cold-dry) conditions, and its onset can be dated to the late 1970s.
- The trends detected in the $\langle IR \rangle$ indices can be related to the behavior of the EA, NAO, SCAN and WeMO teleconnection patterns. The role of atmospheric dynamics is to modulate the thermodynamic relationship between temperatures and precipitation and to cause the slight shift from warm-dry (cold-wet) to warm-wet (cold-dry) conditions.

These results suggest extending this methodology to other geographical areas to verify its usefulness and limitations in different climatic zones. Using daily maximum and minimum temperatures instead of daily mean temperatures can help to deepen some results (such as the role of the NAO or that of the radiative balance between incident solar radiation and terrestrial radiation). In addition, the use of gridded data can help to deepen in the spatial variability of the index. Based on the IR_t index, the characterization of the physical mechanisms that govern the relationship between temperatures and precipitation, in particular the thermodynamic component and the soil-atmosphere feedback, is an aspect that will be the subject of future works.

Acknowledgements The author wishes to express his gratitude to the anonymous referees for their useful comments.

Author contributions Single autor: study conception and design, material preparation, and analysis were performed by Fernando S. Rodrigo. The manuscript was written by Fernando S. Rodrigo.

Funding The author declares that no funds, grants, or other support were received during the preparation of this manuscript.

Data availability Temperature and precipitation data analysed during the current study are available in the European Climate Assessment & Dataset Project (ECA&D; <https://www.ecad.eu/dailydata/index.php>); EA, EA/WR, NAO, and SCAN indices data are from the Climate Prediction Center (<http://www.ncep.noaa.gov/teledoc>) and the WeMO index is from the Climate Research Unit, University of East Anglia (<http://cru.aec.uk>).

Declarations

Competing interests Author declares he has no financial interests.

References

- Adler RF, Gu G, Wang J-J, Huffman GJ, Curtis S, Bolvin D (2008) Relationships between global precipitation and surface temperature on interannual and longer timescales (1979–2006). *J Geophys Res* 113:D22104. <https://doi.org/10.1029/2008JD010536>
- Alexander LV, Zhang X, Peterson TC, Caesar J, Gleason B, Klein Tank AMG, Haylock M, Collins D, TrewinRahimzadeh BF, Tagipour A, Rupa Kumar K, Revadekar J, GriffithsVincent GL, Stephenson DB, Burn J, Aguilar E, Brunet M, Taylor M, New M, Zhai P, Rusticucci M, Vazquez-Aguirre JL (2006) Global observed changes in daily climate extremes of temperature and precipitation. *J Geophys Res* 111:D05109. <https://doi.org/10.1029/2005JD006290.2006>
- Alley RB, Marotzke J, Nordhaus WD, Overpeck JT, Peteet DM, Pielke RA, Pierrehumbert RT, Rhines PB, Stocker TF, Talley LD, Wallace JM (2003) Abrupt climate change. *Science* 299:2005–2010. <https://doi.org/10.1126/science.1081056>
- Barnston AG, Livezey RE (1987) Classification, seasonality and persistence of low-frequency atmospheric circulation patterns. *Mon Weather Rev* 115:1083–1126. [https://doi.org/10.1175/1520-0493\(1987\)115%3c1083:CSAPOL%3e2.0.CO;2](https://doi.org/10.1175/1520-0493(1987)115%3c1083:CSAPOL%3e2.0.CO;2)
- Beniston M (2009) Decadal-scale changes in the tails of probability distribution functions of climate variables in Switzerland. *Int J Climatol* 29:1362–1368. <https://doi.org/10.1002/joc.1793>
- Berg P, Haerter JO, Thejll P, Piani C, Hagemann S, Christensen JH (2009) Seasonal characteristics of the relationship between daily precipitation intensity and surface temperature. *J Geophys Res* 114:D18102. <https://doi.org/10.1029/2009JD012008>
- Berg P, Lintner BR, Findell K, Seneviratne SI, Van der Hurk B, Ducharme A, Cghéry F, Hagemann S, Lawrence DM, Malyshev S, Meier A, Gentile P (2015) Interannual coupling between summertime surface temperature and precipitation over land: processes and implications for climate change. *J Clim* 28:1308–1328. <https://doi.org/10.1175/JCLI-D-14-00324.1>
- Blöschl G, Kiss A, Viglione A, Barriendos M, Böhm O, Brázdil R, Coeur D, Demarée G, Llasat MC, Macdonald N, Retsö D, Roald L, Schmocker-Fackel P, Amorim I, Bělnová M, Benito G, Bertolin C, Camuffo D, Cornel D, Doktor R, Elleder L, Enzi S, Garcia JC, Glaser R, Hall J, Haslinger K, Hofstätter M, Komma J, Limanówka D, David D, Panin A, Parajka J, Petrić H, Rodrigo FS, Rohr C, Schönbein J, Schulte L, Silva LP, Toonen WHJ, Valent P, Waser J, Wetter O (2020) Current European flood-rich period exceptional compared with past 500 years. *Nature* 583:560–566. <https://doi.org/10.1038/s41586-020-2478-3>
- Calmanti S, Dell'Aquila A, Maimone F, Pelino V (2015) Evaluation of climate patterns in a regional climate model over Italy using long-term records from SYNOP weather stations and cluster analysis. *Clim Res* 62:173–188. <https://doi.org/10.3354/cr01256>
- Chen W, Cui H, Ge Q (2022) The spatial and seasonal dependency of daily precipitation extremes on the temperature in China from 1957 to 2017. *Int J Climatol* 42(3):1560–1575. <https://doi.org/10.1002/joc.7320>
- Cheng L, Hoerling M, Smith L, Eischeid J (2018) Diagnosing Human-Induced Dynamic and Thermodynamic Drivers of Extreme Rainfall. *J Climate* 31:1029–1051. <https://doi.org/10.1175/JCLI-D-16-0919.1>
- Cong R-G, Brady M (2012) The interdependence between rainfall and temperature: copula analyses. *Sci World J* 2012(405675):11. <https://doi.org/10.1100/2012/405675>
- Crhová L, Holtanová E (2018) Simulated relationship between air temperature and precipitation over Europe: sensitivity to the choice of RCM and GCM. *Int J Climatol* 38:1595–1604. <https://doi.org/10.1002/joc.5256>
- Dobrinsky P, Da Silva N, Panthou G, Bastin S, Muller C, Ahrens B, Borge M, Conte D, Fossier G, Giorgi F, Güntler I, Kotroni V, Li L, Morin E, Öno B, Quintana-Seguí P, Romera R, Zsolt Torma C (2018) Scaling precipitation extremes with temperature in the Mediterranean: past climate assessment and projection in anthropogenic scenarios. *Clim Dyn* 51:1237–1257. <https://doi.org/10.1007/s00382-016-3083-x>
- Dong H, Huang S, Fang W, Leng G, Yang H, Ren K, Zhao J, Ma C (2021) Copula-based non-stationarity detection of the precipitation-temperature dependency structure dynamics and possible driving mechanism. *Atmos Res* 249:105280. <https://doi.org/10.1016/j.atmosres.2020.105280>
- Du H, Wu Z, Jin Y, Zong S, Meng X (2013) Quantitative relationships between precipitation and temperature over Northeast China, 1961–2010. *Theor Appl Climatol* 113:659–670. <https://doi.org/10.1007/s00704-012-0815-7>
- El Kenawy A, López-Moreno JJ, Viicente-Serrano SM (2012) Trend and variability of surface air temperature in northeastern Spain (1920–2006): Linkage to atmospheric circulation. *Atmos Res* 106:159–180. <https://doi.org/10.1016/j.atmos.res.2011.12.006>
- Falquina R, Gallardo C (2017) Development and application of a technique for projecting novel and disappearing climates using cluster analysis. *Atmos Res* 197:224–231. <https://doi.org/10.1016/j.atmosres.2017.06.031>
- Fernández-Montes S, Rodrigo FS (2012) Trends in seasonal indices of daily temperature extremes in the Iberian Peninsula, 1929–2005. *Int J Climatol* 32:2320–2332. <https://doi.org/10.1002/joc.3399>
- Fernández-Montes S, Gómez-Navarro JJ, Rodrigo FS, García-Valero JA, Montávez JP (2017) Covariability of seasonal temperature and precipitation over the Iberian Peninsula in high-resolution climate simulations (1001–2099). *Planet. Change*, in press, Glob. <https://doi.org/10.1016/j.gloplacha.2016.09.007>
- Giorgi F (2008) A simple equation for regional climate change and associated uncertainty. *J Climate* 21:1589–1604. <https://doi.org/10.1175/2007JCLI1763.1>
- González Reviriego N, Rodríguez Puebla C, Belén Rodríguez F (2014) Evaluation of teleconnections over the Euro-Atlantic region on the basis of Partial Least Squared regression. *Clim Dyn* 44:2989–3014. <https://doi.org/10.1007/s00382-014-2367-2>
- Hall RJ, Hanna E (2018) North Atlantic circulation indices: links with summer and winter UK temperature and precipitation and

- implications for seasonal forecasting. *Int J Climatol* 38:660–677. <https://doi.org/10.1002/joc.5398>
- Hao Z, Zhang X, Singh VP, Hao F (2020) Joint modeling of precipitation and temperature under influences of El Niño Southern Oscillation for compound event evaluation and prediction. *Atmos Res* 245:105090. <https://doi.org/10.1016/j.atmosres.2020.105090>
- Hare SR, Mantua NJ (2000) Empirical evidence for North Pacific regime shifts in 1977 and 1989. *Prog Oceanogr* 47(2–4):103–145. [https://doi.org/10.1016/S0079-6611\(00\)00033-1](https://doi.org/10.1016/S0079-6611(00)00033-1)
- Hurrell JW, Kushnir Y, Ottersen G, Visbeck M (2003) An overview of the North Atlantic Oscillation. In: Hurrell JW, Kushnir Y, Ottersen G, Visbeck M (eds) *The North Atlantic Oscillation: climatic significance and environmental impact*. American Geophysical Union, Washington, pp 51–62
- Isaac GA, Stuart RA (1992) Temperature-Precipitation Relationships for Canadian Stations. *J Climate* 5:822–830. [https://doi.org/10.1175/1520-0442\(1992\)005%3c0822:TRFCS%3e2.0.CO;2](https://doi.org/10.1175/1520-0442(1992)005%3c0822:TRFCS%3e2.0.CO;2)
- Ivanov MA, Evtimov SN (2010) 1963: The break point of the Northern Hemisphere temperature trend during the twentieth century. *Int J Climatol* 30:1738–1746. <https://doi.org/10.1002/joc.2002>
- Joliffe IT, Philipp A (2010) Some recent developments in cluster analysis. *Phys Chem Earth* 35:309–315. <https://doi.org/10.1016/j.pce.2009.07.014>
- Kim JU, Boo K-O, Shim S, Kwon W-T, Byun Y-H (2017) The Seasonal Correlation Between Temperature and Precipitation Over Korea and Europe and the Future Change From RCP8.5 Scenario. *Atmosphere*. Korean Meteorological Society 27:79–91. <https://doi.org/10.14191/Atmos.2017.27.1.079Kim2017>
- Klein-Tank AMG et al (2002) Daily dataset of 20th-century surface air temperature and precipitation series for the European climate assessment. *Int J Climatol* 22:1441–1453. <https://doi.org/10.1002/joc.773>
- Lazoglou G, Anagnostopoulou C (2019) Joint distribution of temperature and precipitation in the Mediterranean, using the Copula method. *Theor Appl Climatol* 135:1399–1411. <https://doi.org/10.1007/s00704-018-2447-z>
- López-Bustins JA, Martín-Vide J, Sánchez-Lorenzo A (2008) Iberia winter rainfall trends based upon changes in teleconnection and circulation patterns. *Glob Planet Change* 63:171–176. <https://doi.org/10.1016/j.gloplacha.2007.09.002>
- Mahlstein I, Knutti R (2010) Regional climate change patterns identified by cluster analysis. *Clim Dyn* 35:587–600. <https://doi.org/10.1007/s00382-009-0654-0>
- Manzano AM, Clemente MA, Morata A, Luna MY, Beguería S, Vicente-Serrano SM, Martín ML (2019) Analysis of the atmospheric circulation pattern effects over SPEI drought index in Spain. *Atmos. Res.* 230:104630. <https://doi.org/10.1016/j.atmosres.2019.104630>
- Martín Vide J, Olecina CJ (2001) *Climas y tiempos de España*. Alianza Editorial, Madrid
- Martín-Vide J, López-Bustins JA (2006) The Western Mediterranean Oscillation and rainfall in the Iberian Peninsula. *Int J Climatol* 26:1455–1475. <https://doi.org/10.1002/joc.1388>
- Merino A, Martín ML, Fernández-González S, Sánchez JL, Valero F (2018) Extreme maximum temperature events and their relationships with large-scale modes: potential hazard on the Iberian Peninsula. *Theor Appl Climatol* 133:531–550. <https://doi.org/10.1007/s00707-017-2203-9>
- Muñoz-Díaz D, Rodrigo FS (2004) Spatio-temporal patterns of seasonal rainfall in Spain (1912–2000) using cluster and principal component analysis: comparison. *Annales Geophysicae* 22:1435–1448 (432-0576/ag/2004-22-1435)
- Nojarov P (2017) Genetic climatic regionalization of the Balkan Peninsula using cluster analysis. *J Geogr Sci* 27:43–61. <https://doi.org/10.1007/s11442-017-1363-y>
- Philipp A, Della-Marta PM, Jacobeit J, Fereday DR, Jones PD, Moberg A, Wanner H (2007) Long-term variability of daily North-Atlantic-European pressure patterns since 1850 classified by simulated annealing clustering. *J Climate* 20:4065–4095. <https://doi.org/10.1175/JCLI4175.1>
- Pinskwar I (2022) Complex changes of extreme precipitation in the warming climate of Poland. *Int J Climatol* 42:817–833. <https://doi.org/10.1002/joc.7274>
- Ramos AM, Trigo RM, Liberato MLR (2014) A ranking of high-resolution daily precipitation extreme events for the Iberian Peninsula. *Atmos. Sci Lett* 2014:1–7. <https://doi.org/10.1002/asl2.507>
- Ríos-Cornejo D, Penas A, Álvarez-Esteban R, del Río S (2015) Links between teleconnection patterns and mean temperature in Spain. *Theor Appl Climatol* 122:1–18. <https://doi.org/10.1007/s00704-014-1256-2>
- Rodrigo FS (2019) Coherent variability between seasonal temperatures and rainfalls in the Iberian Peninsula, 1951–2016. *Theor Appl Climatol* 135:473–490. <https://doi.org/10.1007/s00704-018-2400-1>
- Rodrigo FS (2022) A simple approach for the study of the relationship between temperature and precipitation. *Theor Appl Climatol* 150:215–228. <https://doi.org/10.1007/s00704-022-04154-w>
- Ruiz-Leo AM, Hernández E, Queralt S, Maqueda G (2013) Convective and stratiform precipitation trends in the Spanish Mediterranean coast. *Atmos Res* 119:46–55. <https://doi.org/10.1016/j.atmosres.2011.07.019>
- Rust HW, Richling A, Bissolli P, Ulbrich U (2015) Linking teleconnection patterns to European temperature- a multiple linear regression model. *Meteorol Z* 24:411–423. <https://doi.org/10.1127/metz/2015/0642>
- Sa'adi Z, Shahid S, Sanusi Shiru M (2021) Defining climate zone of Borneo based on cluster analysis. *Theor and App Climatol* 145:1467–1484. <https://doi.org/10.1007/s00704-021-03701-1>
- Savin NE, White KJ (1977) The Durbin-Watson Test for Serial Correlation with Extreme Sample Sizes or Many Regressors. *Econometrica* 45:1989–1996
- Siraj-Ud-Douh NI (2019) Defining homogeneous climate zones of Bangladesh using cluster analysis. *Int J Stat Math* 6:119–129
- Stuart RA, Isaac GA (1994) A comparison of temperature-precipitation relationships from observations and as modeled by the General Circulation Model of the Canadian Climate Centre. *J Climate* 7:277–282. [https://doi.org/10.1175/1520-0442\(1994\)007%3c0277:ACOTRF%3e2.0.CO;2](https://doi.org/10.1175/1520-0442(1994)007%3c0277:ACOTRF%3e2.0.CO;2)
- Suarez-Gutierrez L, Müller WA, Li C, Marotzke J (2020) Dynamical and thermodynamical drivers of variability in European summer heat extremes. *Clim Dyn* 54:4351–4366. <https://doi.org/10.1007/s00382-020-05233-2>
- Teodoro PE, Oliverira-Júnior JF, Rodrigues da Cunha E, Guedes Correa CC, Torres FE, Matheus Bacani V, Gois G, Pereira Ribeiro L (2016) Cluster analysis applied to the spatial and temporal variability of monthly rainfall in Mato Grosso do Sul State, Brazil. *Meteorol Atmos Phys* 128:197–209. <https://doi.org/10.1007/s00703-015-0408-y>
- Trenberth KE (2011) Changes in precipitation with climate change. *Clim Res* 47:123–138. <https://doi.org/10.3354/cr00953>
- Trenberth KE (2022) *The changing flow of energy through the climate system*. Cambridge University Press, Cambridge
- Trenberth KE, Shea DJ (2005) Relationships between precipitation and surface temperature. *Geophys Res Lett* 32:L14703. <https://doi.org/10.1029/2005GL022760>
- Trigo RM, Osborn TJ, Corte-Real JM (2002) The North Atlantic Oscillation influence on Europe: climate impacts and associated physical mechanisms. *Clim Res* 20:9–17. <https://doi.org/10.3354/cr020009>
- Ullah H, Akbar M, Khan F (2020) Construction of homogeneous climatic regions by combining cluster analysis and L-moment approach on the basis of Reconnaissance Drought Index for

- Pakistan. *Int J Climatol* 40:324–341. <https://doi.org/10.1002/joc.6214>
- van Haren R, Haarsma RJ, de Vries H, van Oldenborgh GJ, Hazeleger W (2015) Resolution dependence of circulation forced future central European summer drying. *Environ. Res. Lett.* 10:055002. <https://doi.org/10.1088/1748-9326/10/5/055002>
- von Storch H, Zwiers FW (1999) *Statistical analysis in climate research*. Cambridge University Press, Cambridge, p 484. <https://doi.org/10.1017/CBO9780511612336>
- Ward JH (1963) Hierarchical grouping to optimize an objective function. *J Am Stat Assoc* 58:236–244. <https://doi.org/10.1080/01621459.1963.10500845>
- Wilks DS (2019) *Statistical methods in the atmospheric sciences*. Academic Press, San Diego
- Wu LY (2014) Changes in the covariability of surface air temperature and precipitation over East Asia associated with climate shift in the late 1970s. *Atmos Ocean Sci Lett* 7:92–97
- Yang J, Zhang Q, Lu G, Liu X, Wang Y, Wang D, LiuW YP, Zhu B, Duan X (2021) Climate Transition from Warm-Dry to Warm-Wet in Eastern Northwest China. *Atmosphere* 12:548. <https://doi.org/10.3390/atmos12050548>
- Zappa G (2019) Regional Climate Impacts of Future Changes in the Mid-Latitude Atmospheric Circulation: a Storyline View. *Current Clim Change Rep* 5:358–371. <https://doi.org/10.1007/s40641-019-00146-7>
- Zerouali B, Chettih M, Abda Z, Mesbah M, Guimaraes Santos CA, Moura Brasil Neto R (2022) A new regionalization of rainfall patterns based on wavelet transform information and hierarchical cluster analysis in northeastern Algeria. *Theor and App Climatol* 147:1489–1510. <https://doi.org/10.1007/s00704-021-03883-8>
- Zolfaghari F, Khosravi H, Shahriyari A, Jabbari M, Abolhasani A (2019) Hierarchical cluster analysis to identify the homogeneous desertification management units. *PLOS ONE* 14(12):e0226355. <https://doi.org/10.1371/journal.pone.0226355>

Publisher's note Springer Nature remains neutral with regard to jurisdictional claims in published maps and institutional affiliations.

Springer Nature or its licensor (e.g. a society or other partner) holds exclusive rights to this article under a publishing agreement with the author(s) or other rightsholder(s); author self-archiving of the accepted manuscript version of this article is solely governed by the terms of such publishing agreement and applicable law.